The National Severe Storms Laboratory Tornado Detection Algorithm

E. DEWAYNE MITCHELL

NOAA/Environmental Research Laboratories, National Severe Storms Laboratory, and Cooperative Institute for Mesoscale Meteorological Studies, University of Oklahoma, Norman, Oklahoma

STEVEN V. VASILOFF

NOAA/Environmental Research Laboratories, National Severe Storms Laboratory, Norman, Oklahoma

GREGORY J. STUMPF

NOAA/Environmental Research Laboratories, National Severe Storms Laboratory, and Cooperative Institute for Mesoscale Meteorological Studies, University of Oklahoma, Norman, Oklahoma

ARTHUR WITT, MICHAEL D. EILTS, AND J. T. JOHNSON

NOAA/Environmental Research Laboratories, National Severe Storms Laboratory, Norman, Oklahoma

KEVIN W. THOMAS

NOAA/Environmental Research Laboratories, National Severe Storms Laboratory, and Cooperative Institute for Mesoscale Meteorological Studies, University of Oklahoma, Norman, Oklahoma

(Manuscript received 11 March 1997, in final form 4 February 1998)

ABSTRACT

The National Severe Storms Laboratory (NSSL) has developed and tested a tornado detection algorithm (NSSL TDA) that has been designed to identify the locally intense vortices associated with tornadoes using the WSR-88D base velocity data. The NSSL TDA is an improvement over the current Weather Surveillance Radar-1988 Doppler (WSR-88D) Tornadic Vortex Signature Algorithm (88D TVS). The NSSL TDA has been designed to address the relatively low probability of detection (POD) of the 88D TVS algorithm without a high false alarm rate (FAR). Using an independent dataset consisting of 31 tornadoes, the NSSL TDA has a POD of 43%, FAR of 48%, critical success index (CSI) = 31%, and a Heidke skill score (HSS) of 46% compared to the 88D TVS, which has a POD of 3%, FAR of 0%, CSI of 3%, and HSS of 0%. In contrast to the 88D TVS, the NSSL TDA identifies tornadic vortices by 1) searching for strong shear between velocity gates that are azimuthally adjacent and constant in range, and 2) not requiring the presence of an algorithm-identified mesocyclone. This manuscript discusses the differences between the NSSL TDA and the 88D TVS and presents a performance comparison between the two algorithms. Strengths and weaknesses of the NSSL TDA and NSSL's future work related to tornado identification using Doppler radar are also discussed.

1. Introduction

The capability to effectively warn the public and aviation community of severe and hazardous weather is a crucial mission of the National Weather Service (NWS) and the Federal Aviation Administration (FAA). It is imperative to both the NWS and FAA that such weather phenomena such as large hail, damaging winds, tornadoes, lightning, and flash floods be anticipated and identified. Many tools have been developed and implemented to help anticipate and diagnose these weather phenomena. One such tool is the Weather Surveillance Radar-1988 Doppler (WSR-88D) (Klazura and Imy 1993; Crum and Alberty 1993). This relatively new tool has enabled NWS forecasters to better anticipate and identify severe and hazardous events. It has been reported that the use of the WSR-88D has improved the timeliness and accuracy of severe thunderstorm and tornado warnings (Polger et al. 1994; Bieringer and Ray 1996). In recent years, a significant rise in the probability of detection (POD) as well as a decrease in the false alarm rate (FAR) has occurred with the advent and use of the WSR-88D. Also, Polger et al. (1994) presented evidence that the various products available (e.g., base data displays, algorithm output, etc.) via the WSR-

Corresponding author address: E. DeWayne Mitchell, NOAA/ERL/NSSL, 1313 Halley Circle, Norman, OK 73069.
E-mail: mitchell@nssl.noaa.edu

88D have helped forecasters determine whether the public should be warned of severe and/or tornadic weather.

The concept of severe thunderstorm and tornado detection using Doppler radar was born over four decades ago. The pioneering efforts of Browning (1965), Easterbrook (1967), Lhermitte (1969), and Donaldson (1970) laid a foundation for the recognition of potentially tornadic thunderstorms using Doppler radar. By using conventional incoherent radar, they inferred motion within storms via the redistribution of precipitation echoes. Probably the first demonstration of the potential for Doppler radar to identify tornadic vortices occurred in 1958 when the Eldorado, Kansas, tornado was scanned using a 3-cm continuous wave Doppler radar (Smith and Holmes 1961). However, continuous wave Doppler radar technology was deemed inadequate to properly diagnose tornadic vortices in part because range information could not be determined. As a result, the development of improved remote sensing techniques using pulsed Doppler radar to observe storm-scale air motions was pursued.

Prior to the use of Doppler radar, the identification of potentially tornadic storms was accomplished by identifying the hook echo or the ''figure 6'' echo with the use of an incoherent radar. These features, now quite familiar, have been described as protrusions within a reflectivity field emanating from the rear flank of a convective storm. The identification of this feature was first documented by Austin (1945). However, the significance of this feature was not fully realized until a hook echo was observed in association with an Illinois tornado (Stout and Huff 1953; Fujita 1958). Afterward, this signature was often noted to be associated with tornadoes (Bigler 1955, 1956; Wells 1963; Freund 1966; Sadowski 1969). Later, hook echoes were described by Browning (1965) as echoes resulting from the redistribution of precipitation by air motions within a storm.

Even though the hook echo appeared promising as a definitive signature for tornadic storms, it was determined to not be completely reliable. Forbes (1981), in an attempt to quantify the accuracy of the hook echo as an indicator of tornadic storms using weather radar, used a dataset consisting of tornadoes that occurred during the 3 April 1974 ''superoutbreak'' and determined that not all of the tornadic storms exhibited a characteristic hook echo or any other distinctive reflectivity echo. However, it was noted that 65% of the distinctive echoes were tornadic, encompassing 81% of the tornadoes. Furthermore, it was determined that the appearance of a hook echo or other distinctive echo did not provide sufficient lead time for tornado warnings and that a high false alarm rate may occur. Instead, Forbes (1981) concluded that pulsed Doppler radar's capability to sample potentially tornadic vortices would be a vast improvement over incoherent radar technology to identify storms that had the potential of becoming tornadic.

Improvements in pulsed Doppler radar technology during the 1960s and early 1970s led to discoveries that are still used today in operational meteorology. The first pulsed Doppler radar measurements of a developing hook echo were made by Brown et al. (1971). A strong azimuthal velocity gradient was observed coincident with the developing hook echo. Later, the first pulsed Doppler radar observation of a tornado was made during the Brookline, Massachusetts, tornado on 9 April 1972 (Kraus 1973). Interestingly, no hook echo was observed at the time of the tornado; however, a hook echo was observed prior to tornadogenesis. In 1973, the National Severe Storms Laboratory's 10-cm pulsed Doppler radar scanned through a tornadic thunderstorm near Union City, Oklahoma, and revealed strong gate-to-gate (adjacent in azimuth and constant in range) velocity differences 25 min prior to and during the occurrence of a tornado (Burgess et al. 1975; Brown et al. 1978). This signature, now commonly known as the tornadic vortex signature (TVS), appeared to develop at midaltitudes within the storm and descend toward the surface over time. Furthermore, the azimuthal shear associated with the signature often exceeded 0.01 s^{-1}. Brown et al. (1978) noted that the TVS in the Union City storm, as well as in other observed tornadic storms, was characterized by vertical continuity and persistence in time. This observation was pivotal in that it solidified earlier suggestions that tornadoes could be inferred by close-proximity velocity extrema using pulsed Doppler radar.

One shortcoming in vortex recognition using Doppler radar is the broadening of the radar beam with increased range from the radar (Zrnic and Doviak 1975; Brown et al. 1978). As the width of the radar beam increases with range, the observed velocity peaks associated with a given vortex decrease in magnitude. Thus, some tornadoes, in particular weak tornadoes, may escape identification using the WSR-88D, even at close ranges ($<$20 km) (Burgess et al. 1993; Vasiloff 1993). This fact poses a significant challenge to automated vortex recognition (Burgess et al. 1993; Wakimoto and Lew 1993; Mitchell and Stumpf 1996) especially since, at the time of occurrence, the size of the vortex is unknown. Recently, Wood and Brown (1997) have shown quantitatively, by mimicking the discrete sampling of the WSR-88D, that the appearance of a given TVS or mesocyclone may change significantly by the random positioning of the radar beam center relative to the center of a simulated vortex. The random sampling of a vortex by pulsed Doppler radar may have significant effects on derived vortex measures (e.g., rotational velocity, shear, and depth). As a result, the apparent trend of tornadic vortex characteristics and evolution may be a function of storm evolution, storm motion, and/or discrete radar sampling (both horizontal and vertical). Thus, forecasters must be judicious in their decision making in a severe weather warning situation using trend information (Howard et al. 1997).

Nevertheless, historical observations of TVSs provide a framework for the design of the operational WSR-

88D TVS algorithm (Crum and Alberty 1993). Since 1990, the National Severe Storms Laboratory (NSSL), in cooperation with the FAA and the NWS Operational Support Facility (OSF), has developed and tested the NSSL Tornado Detection Algorithm (hereafter, NSSL TDA). The deployment of the WSR-88D, along with the ability to record the Doppler moment data, has made it possible to examine a larger number of cases from various regions, seasons, and near-storm environments across the United States for the development of improved severe weather detection algorithms. To date, the NSSL TDA has been developed and tested using recorded WSR-88D base data as well as in real time by NWS operational warning forecasters (Johnson et al. 1995; Stumpf and Foster 1996)

The current WSR-88D TVS algorithm (hereafter, 88D TVS) has a very low POD (<5%) and FAR (<5%) (Vasiloff 1992; Mitchell 1995). The NSSL TDA has been designed to address the extremely low POD of tornadoes by the 88D TVS without an extremely high FAR. Furthermore, and perhaps more importantly, the NSSL TDA has been designed to provide the forecaster with insightful diagnostic information regarding potentially tornadic vortices.

A description of the NSSL TDA-is provided in section 2. Section 3 compares the functions of the NSSL TDA and the 88D TVS. Section 4 discusses a performance evaluation of the NSSL TDA and the 88D TVS and compares the scores of each algorithm. An evaluation summary of the NSSL TDA and the 88D TVS is discussed in section 5. Finally, concluding remarks and future work are presented in section 6.

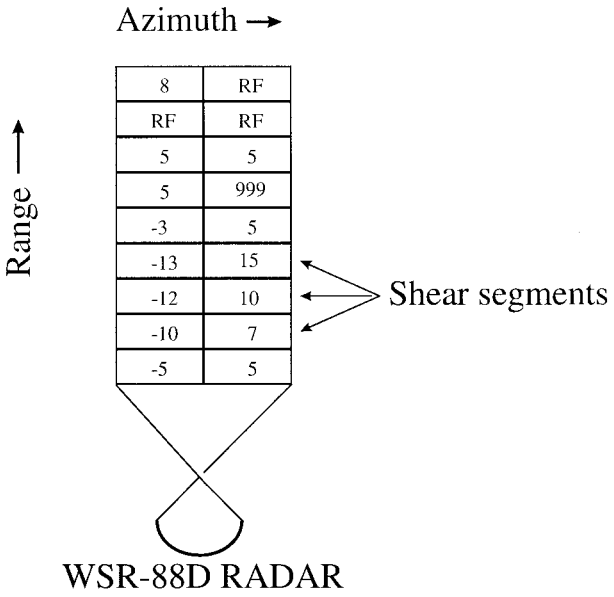

FIG. 1. Shear segment processing by the NSSL TDA. Each pair of azimuthally adjacent velocity gates is examined in increasing range order. Range and azimuth increase toward the top and the right of the figure, respectively. Outbound and inbound velocities are noted by positive and negative velocity values, respectively. RF represents range-folded echoes while 999 represents missing data. The shear segments satisfying the minimum velocity difference threshold of 11 m s^{-1} are indicated.

2. NSSL TDA description

a. Functional overview

The NSSL TDA is designed to examine the velocity difference between adjacent velocity gate pairs at constant range and at each radar elevation angle, within a specified range (e.g., 150 km) from the radar, and below a specified height above radar level (ARL) (e.g., 10 km). Figure 1 illustrates this initial process within the NSSL TDA. Typically, those velocity data with corresponding reflectivity values at or below 0 dBZ are not considered, and the next pair of velocity gates at the next range from the radar are considered. Also, if any velocity data are obscured by range-folded echoes or are missing, then the process continues at the next range gate. The velocity difference between all adjacent velocity gates at the same range is computed as well as the height of the velocity pair. If the velocity difference exceeds a specified adaptable threshold (e.g. 11 m s^{-1}), then the velocity pair is saved as a shear segment and the following attributes are saved: beginning and ending azimuth (°), velocity difference (m s^{-1}), shear ($s^{-1} \times 1000$), range (km), and height ARL (km). This process is repeated until all velocity data within a radar elevation scan have been considered and all shear segments exceeding the minimum velocity difference threshold have been found.

Once a radar elevation scan has been examined for any shear segments, then 2D features are constructed for each radar elevation angle. The process of constructing 2D features uses six velocity difference thresholds in the following order: 35, 30, 25, 20, 15, and 11 m s^{-1}. This technique of using multiple thresholds allows the NSSL TDA to isolate core vortices that may be embedded within regions of long azimuthal shear (e.g., radially oriented squall lines).

The multiple thresholding process begins by considering only those shear segments that exceed the largest velocity difference criterion (e.g., 35 m s^{-1}). A 2D feature is comprised of at least three shear segments, and the centroid of each shear segment must lie within 1.0° azimuthal distance and 500-m radial distance (each are adaptable parameters) of its immediate neighbor(s). An example of a 2D feature is shown in Fig. 2 for an actual tornado event. Additional processing is done to ensure that only one shear segment remains at each range within a 2D feature and that no shear segment is used in more than one 2D feature. Once all shear segments have been considered during the construction of a given 2D feature, the process continues until all 2D features have been found. An aspect ratio (radial extent/azimuthal extent) is computed for each 2D feature, and if the aspect ratio exceeds a defined threshold (currently set to four)

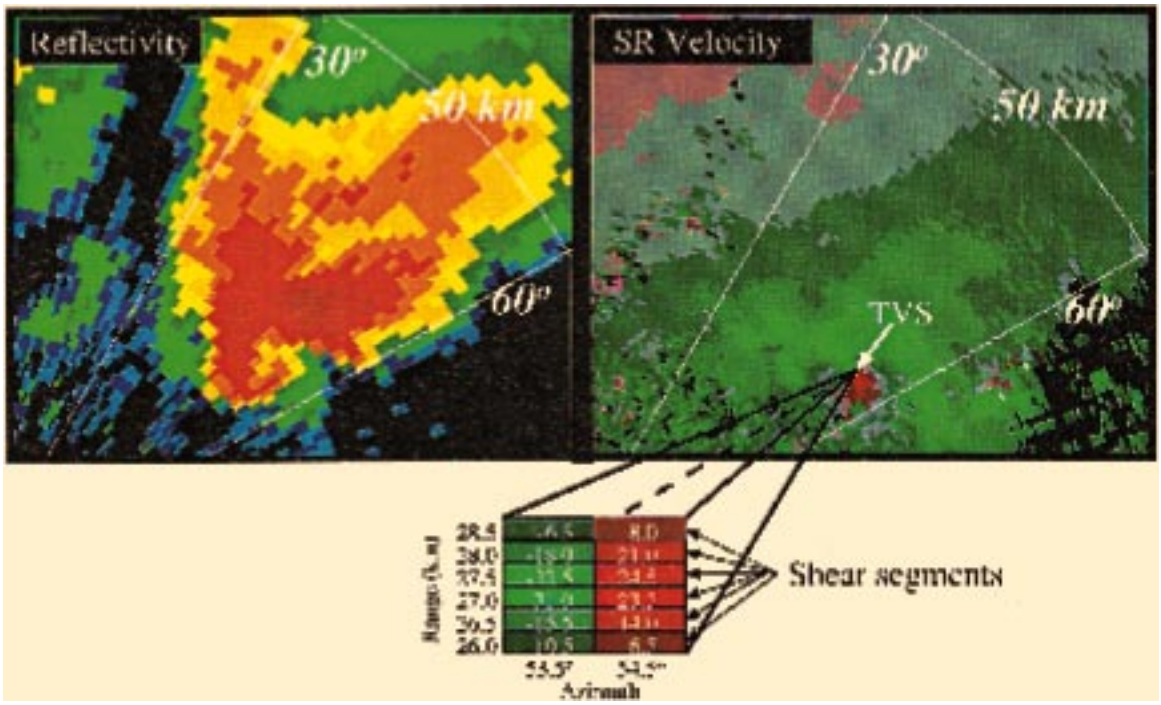

FIG. 2. Images of reflectivity and velocity images of a tornadic supercell captured by the Aberdeen, South Dakota, WSR-88D at 2320 UTC 31 May 1996 at 0.5°. The TVS is indicated on the storm-relative (SR) velocity image. The TVS is enlarged below the radar images to reveal individual velocity data gates and their values. Each azimuthally adjacent pair of velocity gates represents a shear segment. The positive and negative velocity values indicate outbound and inbound velocity values, respectively.

then the 2D feature is discarded. The aspect ratio check is incorporated to avoid identification of azimuthal shear regions such as gust fronts. At this juncture, all remaining 2D features are deemed 2D detections, and the center azimuth (°), center range (km), maximum velocity difference (m s^{-1}), maximum shear ($s^{-1} \times 1000$), and altitude ARL (km) are saved. The entire process described above is repeated for each successively lower velocity difference threshold. However, if a 2D detection from a lower velocity difference threshold overlaps only one 2D detection with a higher velocity difference threshold, then the overlapping 2D detection is saved. If two or more 2D detections from a higher velocity difference threshold are overlapped, then the 2D detection from the lower velocity difference threshold is discarded (Fig. 3). In this manner, core vortices are identified and retained for later processing.

Vertical continuity is then examined once all 2D detections have been identified for every radar elevation scan within an entire volume scan. A 3D feature is required to comprise at least two 2D detections, and, ideally, no gaps between vertically neighboring 2D detections will occur (Fig. 4). However, a gap may occur if a vortex is obscured by improper velocity dealiasing, range folding, or an apparently weak vortex did not pass the prescribed thresholds during the 2D feature construction process. Therefore, the NSSL TDA allows up to a single elevation angle to separate vertically adjacent 2D detections. Furthermore, the center of each 2D detection is constrained to lie within a horizontal distance of 2.5 km of its vertically adjacent neighbor(s) centroid. All 3D features composed of three or more 2D detections are deemed 3D detections at this point. Each 3D detection is then classified into two categories: TVS and elevated TVS (ETVS). A 3D detection is classified as a TVS if it meets minimum strength and depth criteria and if the base of the 3D detection extends to the 0.5° elevation angle or a prescribed altitude ARL (currently 600 m). Otherwise, a 3D detection that meets the TVS criteria except for the base elevation or altitude criterion is deemed an ETVS. The definition of a TVS here is different from that in the 88D TVS, where a TVS is based primarily upon a more stringent shear criterion. This difference will be discussed in more detail in section 3. Time continuity is not imposed upon any 3D detection for the purpose of classification. Once the 3D detections are classified, the following attributes are saved: maximum gate-to-gate velocity difference (m s^{-1}) at the base of the detection, maximum gate-to-gate velocity difference (m s^{-1}) among all 2D detections and its altitude (km), azimuth (°), range (km), altitude of the 3D detection base (km), maximum shear among all 2D detections ($s^{-1} \times 1000$) and its altitude (km), and detection depth (km). In addition to these attributes, an additional diagnostic measure called the tornado strength index (TSI) is compared for each TVS and ETVS. This measure is calculated by vertically integrating the altitude-weighted maximum gate-to-gate ve-

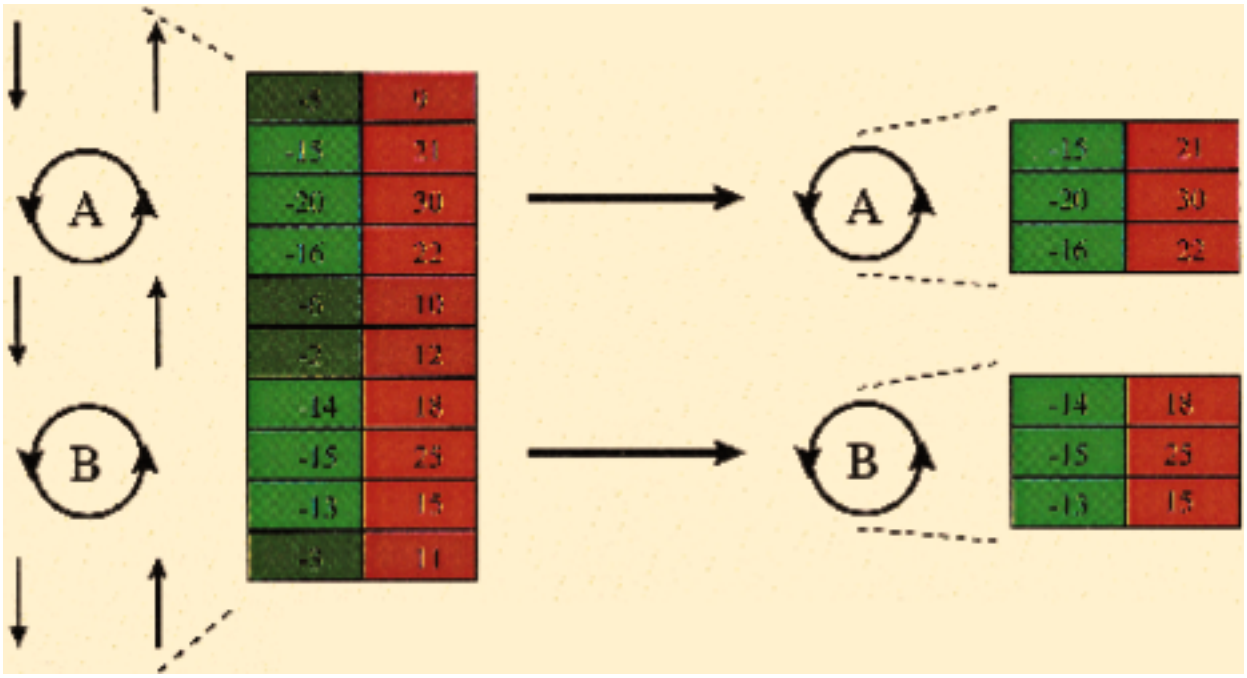

FIG. 3. An example of the 2D detection overlapping process. The core vortices A and B embedded within the larger azimuthal shear region are retained. Each box with inscribed number represents a velocity gate at a given azimuth and range from the radar (located below the page). Each adjacent pair of velocity gates represents a shear segment. Positive and negative velocity values indicate outbound and inbound velocities, respectively.

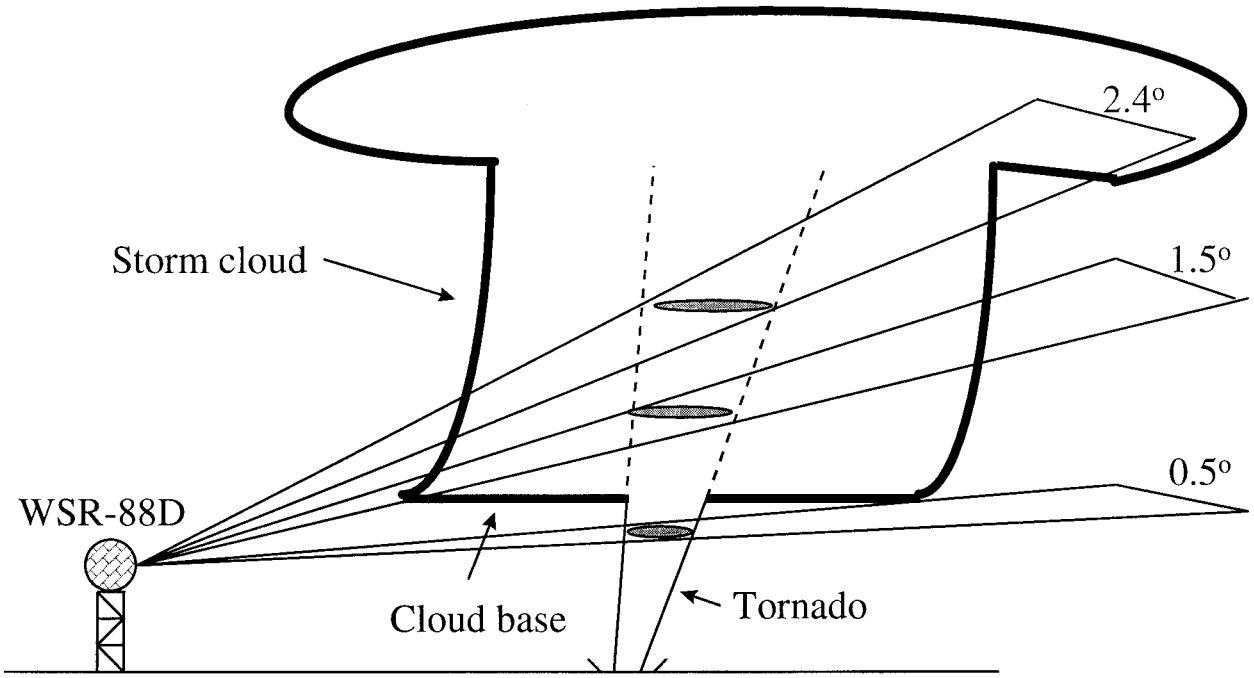

FIG. 4. A schematic of a 3D vortex (dashed and solid cone) composed of three 2D vortices (shaded ellipses). The three lowest WSR-88D elevation angles (0.5°, 1.5°, and 2.4°) are depicted as planes slicing through the 3D vortex.

locity differences of each 2D detection comprising the 3D detection using the trapezoidal rule of the form:

$$\text{TSI} = \int dv\,(H)dH/D$$
$$= [(b - a/2n)(w_1 dv_1 + 2w_2 dv_2 + 2w_3 dv_3 + \cdots 2w_n dv_3 + w_{n+1} dv_{n+1})]/D,$$

where dv = maximum velocity difference within a 2D detection, H = altitude (ARL) of 2D detection, b = altitude (ARL) of detection top, a = altitude (ARL) of detection base, n = number of trapezoid partitions, D = depth of detection, $w = 1$ if $H \leq 3$ km ARL, and $w = 1.4285 - 0.14285(H)$ if $H > 3$ km ARL. It should be noted that a weight of zero is assigned for those detections that are identified at a height of 10 km ARL. The weighting function ranges from 0 to 1 and decreases linearly for all 2D detection altitudes >3 km ARL. The TSI is depth normalized and gives an overall assessment of the vortex by taking depth and strength into account. The reader should be advised that the TSI is still under investigation in terms of its capability to distinguish between tornadic and nontornadic vortices.

b. Tracking and trending of detections

A unique feature of the NSSL TDA is that all 3D detections are tracked and a forecast track is computed. All current TVS or ETVS detection positions are compared to the ''first guess'' forecast positions of the TVS and ETVS detections from the previous volume scan. A graphical representation of the tracking process is presented in Fig. 5. The first guess forecast position is defined as the 5-min forecast position. An expanding search radius technique about a first guess forecast position is employed to determine the most appropriate current detection to associate with the detection from the previous volume scan. Beginning with a 1-km search radius, a search is made for any current detection. If no current detections are found within the 1-km search radius, then the search radius is increased in 1-km increments, up to 10 km, until one or more current detections are found. If more than one current detection is found, then the strongest (i.e., the one with the greatest maximum velocity difference at the detection base) is associated. However, if no current detection is found, then the previous detection is considered ''dead'' and is removed. If a current detection is found, then an intermediate motion vector is computed using the current and previous detection positions. A final motion vector for the time-associated detection is determined by computing the average of the previous and current (intermediate) detection's motion vector (u and v components). At this point, new forecast positions are computed by linearly extrapolating from the current position using the final motion vector. No more than 10 past positions for a given time-associated detection are retained. A maximum of six forecast positions in 5-min intervals are computed for each detection. The number of forecast tracks are constrained to equal the number of past track positions except for those detections that are new or have persisted for more than six volume scans. All unassociated TVSs and/or ETVSs from the current volume scan are assigned a single 5 min forecast position. This forecast position is computed using the average motion vector of all detections from the previous volume scan. However, if no previous detections exist, then either a default motion vector (user specified) is used or the nearest detected storm motion vector derived from the Storm Cell Identification and Tracking (SCIT) algorithm (Johnson et al. 1998).

Finally, the 3D detection attributes for each time-associated detection are saved for the purpose of displaying time trends. Trends can convey to a forecaster valuable information concerning the behavior of potentially tornadic vortices.

An example of the NSSL TDA output using archived radar data from a tornadic event, along with several trends of important diagnostic parameters, is presented in Fig 6. Figure 6 illustrates the output from the NSSL TDA just prior to the occurrence of an F2 tornado that struck near Pond Bank, Pennsylvania, on 30 April 1994. Note that the vortex associated with the tornado was tracked for four consecutive volume scans prior to the tornado, and important information regarding the detection is provided in tables and trend plots.

3. NSSL TDA and 88D TVS functional comparison

Fundamental differences exist between the NSSL TDA and the current 88D TVS. The 88D TVS is inherently based upon the idea that tornadoes are most often associated with supercell storms where a supercell is defined as a deep convective storm characterized by a persistent, rotating updraft or mesocyclone. For the NSSL TDA, this idea has been extended to include nonsupercell tornadoes (Wakimoto and Wilson 1989). The NSSL TDA searches for a TVS regardless of the presence of a mesocyclone.

The current 88D TVS uses a much more stringent shear criterion than the NSSL TDA to identify tornadic vortices. In order for the 88D TVS to be invoked, a mesocyclone must first be identified. Once a mesocyclone is identified, the 88D TVS searches for the inbound and outbound velocity extrema at each elevation angle slicing through the mesocyclone. The search area also includes those velocity data that are within a region around the mesocyclone equal to 5% of the mesocyclone area. If the shear between the velocity extrema exceeds a minimum shear criterion (default = 0.02 s^{-1}) at two or more elevation angles within the mesocyclone, then a TVS is declared. No additional attempt is made to distinguish between tornadic and nontornadic detections. Instead, all TVS detections are considered tornadic. Note that the velocity extrema are not required

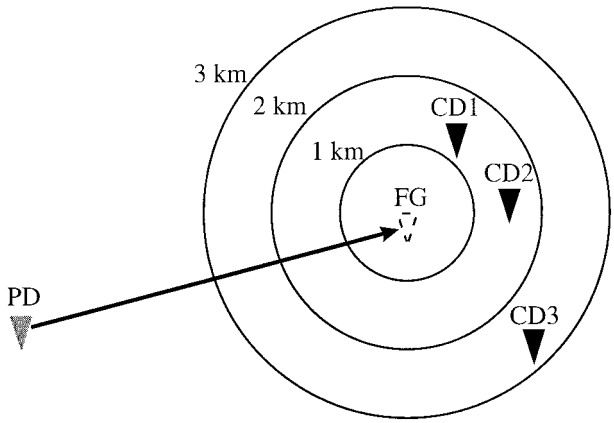

FIG. 5. An example of the NSSL TDA tracking process. The dark inverted triangles depict current detections (CD1, CD2, CD3). The shaded inverted triangle represents a previous detection (PD). The dashed inverted triangle represents the ''first guess'' forecast position (FG). Only three search radii are shown. The strongest detections in rank order are CD1, CD2, and C31. Thus, PD is associated with CD1.

to be adjacent in azimuth and constant in range. As a result of the stringent nature of the 88D TVS, this algorithm produces very few false alarms but is compromised by an extremely low probability of detection. The 88D TVS does not maintain past locations, compute forecast position locations, or maintain time trends of identified TVS characteristics.

By comparison, the NSSL TDA identifies vortices regardless of whether a mesocyclone is detected via examination of gate-to-gate velocities, and is independent of any other algorithm. The NSSL TDA is capable of identifying tornadic vortices that are unaccompanied by mesocyclones such as landspouts (Brady and Szoke 1989) and along the leading edge of squall lines (Stumpf and Burgess 1993). The NSSL TDA uses low velocity difference thresholds to identify locally intense vortices and then attempts to classify them as either tornadic or nontornadic. Perhaps more importantly, the NSSL TDA is capable of 1) tracking persistent tornadic vortices, 2) forecasting their future positions, and 3) producing trends of various vortex measures. In other words, the NSSL TDA provides potentially useful information to the radar operator instead of just providing categorical ''yes, there is a tornado'' or ''no, there is no tornado'' guidance.

4. Algorithm performance evaluation

a. Dataset

The first step in the evaluation process was to define both a dependent and an independent dataset (Tables 1 and 2). The dependent dataset contains 25 tornadoes while 32 tornadoes are contained in the independent dataset. All tornadoes within both datasets occurred within 150 km of a WSR-88D radar in diverse geographical areas of the United States.

The dependent dataset was used as a training dataset to determine and optimize the best set of parameters within the NSSL TDA to discriminate between tornadic and nontornadic vortices. The independent dataset was used to test the NSSL TDA's capability to detect tornadoes based on the chosen set of optimized parameters from the training dataset while all other parameters were held constant. Important NSSL TDA parameters that were used in the performance evaluation are listed in the appendix.

An enhanced version of the WSR-88D velocity dealiasing algorithm was used to dealias the velocity data prior to running the 88D TVS and NSSL TDA. This version of velocity dealiasing included optimized adaptable parameter values necessary to avoid removal of velocity data in problematic regions (Conway et al. 1995).

In the same manner as the NSSL TDA, the 88D TVS was run on both the dependent and independent datasets described above. The 88D TVS was run using the default TVS shear value of 0.02 s^{-1} (default 88D TVS) and then less stringent TVS shear values of 0.005 s^{-1} and 0.01 s^{-1}. It was determined from trial runs using the dependent dataset that a TVS shear value of 0.005 s^{-1} (optimized 88D TVS) was optimum. Only the results using the default and optimized 88D TVS shear values are presented here. Finally, for the 88D TVS, an optimized set of WSR-88D Mesocyclone/TVS Algorithm (88D MTA) site adaptable parameters were used for the optimized 88D TVS runs since the 88D TVS requires a mesocyclone detection from the 88D MTA. The areal search about a mesocyclone signature was increased from 5% to 10% of the mesocyclone area, and the minimum number of required mesocyclone shear segments was lowered from 10 to 6. Other 88D MTA momentum and shear thresholds that were lowered are listed in the appendix.

b. Scoring methodology

The scoring method used ground truth information to determine the location and time of the tornado events. The ground truth sources included *Storm Data* (NCDC 1992–1994) and damage survey reports received from NWS offices. Careful adjustments in time and/or location of tornadoes were often found necessary for tornado reports found in *Storm Data.* The reader is referred to Witt et al. (1998) for a thorough examination regarding discrepancies found within *Storm Data* and issues related to algorithm scoring.

Once the final ground truth data were established, both algorithms were run to determine the number of hits and misses within a specified time window. The scoring method is illustrated in Fig. 7. The time window extends from −20 min prior to the beginning time of the tornado to one volume scan after the ending time of the tornado. This method of scoring is the same as

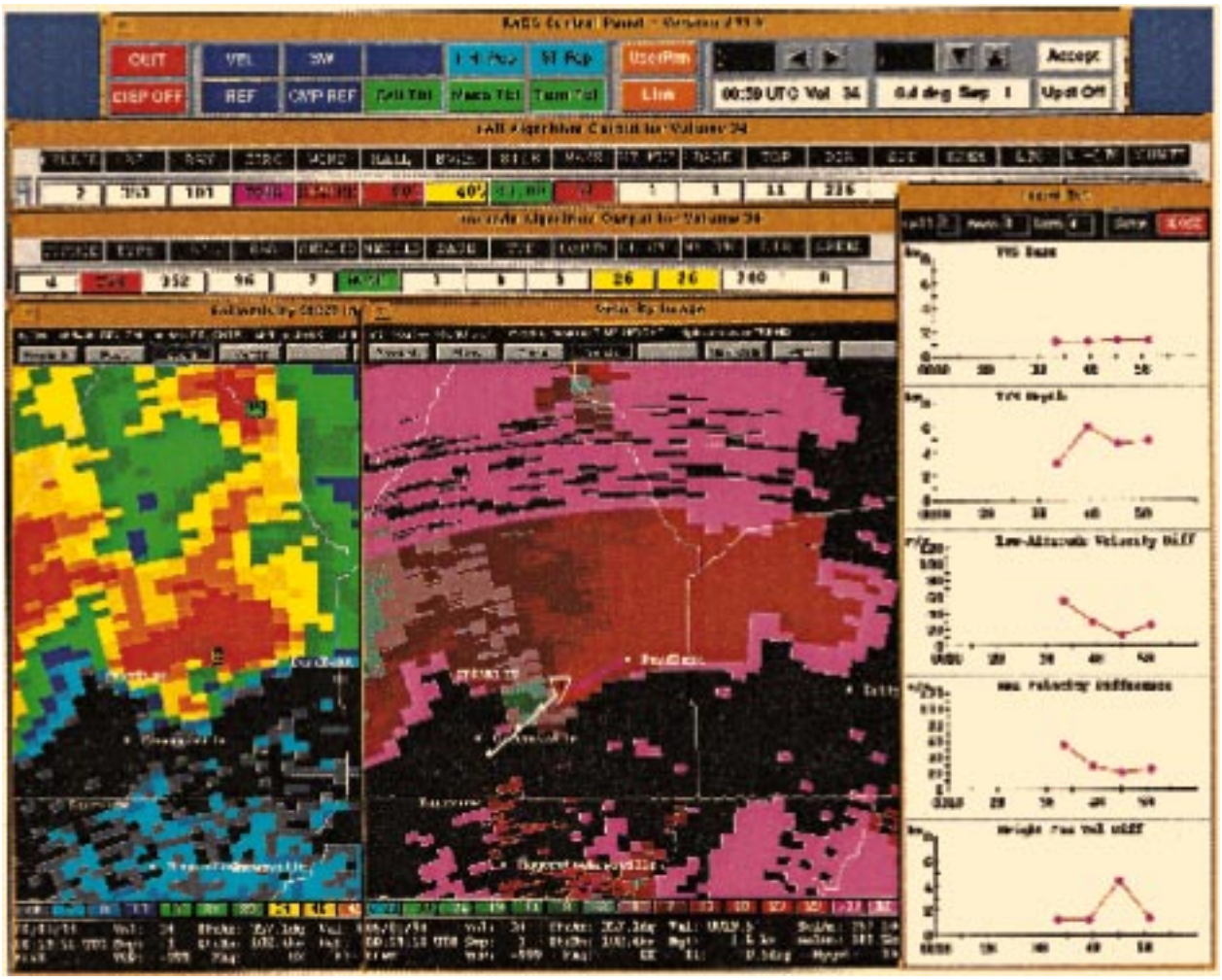

FIG. 6. An example of the NSSL TDA output. Base reflectivity (left) and velocity (right) data are displayed in the lower-left corner and lower center, respectively. The red inverted triangle depicted in the base velocity display represents the current location of a TVS detection with its attendant past (white) and forecast (magenta) track prior to the occurrence of the Pond Bank, PA, tornado on 30 April 1994. Trends as well as tabular output from the NSSL TDA are shown.

that described in Witt et al. (1998). The following definitions apply:

hit: correct detection (per volume scan) during time window,
miss: no detection (per volume scan) during time window,
false alarm: detection (per volume scan) not associated with a tornado event, and
null: no detection (per volume scan) during the time of no tornado event.

The time window scoring method allowed for reasonable lead time for tornadoes as well as errors that

TABLE 1. List of cases composing the *dependent dataset* where No. VS and No. h represent the number of volume scans and the number of hours for each case that was processed by the algorithms.

Date	Radar	No. tornadoes	No. VS/No. h	Event type
15 Apr 1994	Houston, TX	1	74/7.5	Squall line/supercell
16 Apr 1993	Sterling, VA	6	180/17.0	Squall line/supercell
30 Apr 1994	Sterling, VA	2	80/7.75	Bow echo/minisupercell
9 Jun 1994	Memphis, TN	4	62/5.0	Squall line
11 May 1992	Norman, OK	11	60/5.75	Supercell
2 Sep 1992	Norman, OK	1	60/5.5	Isolated supercell
	Total	25	516/48.5	

TABLE 2. Same as Table 1 except for *independent dataset.*

Date	Radar	No. tornadoes	No. VS/No. h	Event type
15 Apr 1994	St. Louis, MO	7	51/5.0	Squall line/embedded supercell
5 May 1993	Dodge City, KS	5	60/57.5	Supercell
27 Nov 1994	Memphis, TN	5	75/6.0	Squall line/embedded supercell
16 Nov 1993	Houston, TX	9	80/8.0	Squall line/supercell
9 Jun 1994	Dodge City, KS	5	92/8.25	Low-topped supercell
28 May 1994	Amarillo, TX	1	65/5.75	Isolated supercell
	Total	32	423/38.75	

may exist within the ground truth even though corrections in the ground truth were attempted. The nulls were tallied using the number of cells detected by the NSSL SCIT algorithm (Johnson et al. 1998). At each volume scan, it was assumed that each hit, miss, and false alarm was associated with a single storm cell. Thus, the number of null detections associated with a null event were determined by subtracting the sum of the hits, misses, and false alarms from the total number of SCIT-detected cells. These null detections represented those storm cells that had no detections from the NSSL TDA or 88D TVS and did not produce a tornado. The following scoring statistics were used (Wilks 1995):
probability of detection:

$$\text{POD} = a/(a + c),$$

false alarm ratio:

$$\text{FAR} = b(a + b),$$

critical success index (CSI):

$$\text{CSI} = a(a + b + c), \quad \text{and}$$

Heidke skill score (HSS):

$$\text{HSS} = [2(ad - bc)]/[(a + c)(c + d) + (a + b)(b + d)],$$

where a, b, c, and d are defined as hits, false alarms, misses, and nulls, respectively. The CSI is commonly used to evaluate NWS forecast skill, and Marzban (1998) has shown that HSS is a good measure of skill.

The method of algorithm scoring presented here may not be optimal. However, for the purpose of comparing the NSSL TDA to the 88D TVS, this scoring method is believed to be adequate.

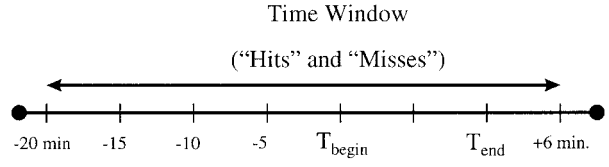

FIG. 7. Schematic of time window scoring method used for scoring the NSSL TDA and the 88D TVS. The time window extends from −20 min prior to the beginning time of the tornado to +6 min after the ending time of the tornado. The beginning (T_{beg}) and ending (T_{end}) time of a tornado event are also indicated.

c. Analysis and scoring

An analysis of the vortices detected by the NSSL TDA showed that of the detection parameters discussed in section 2 three parameters had some skill in distinguishing between tornadic and nontornadic vortices. These parameters were detection depth, maximum gate-to-gate velocity difference at the 0.5° elevation angle, and maximum gate-to-gate velocity difference at any altitude within the 3D detection. Each of the three parameters was varied systematically (i.e., changing the value of one parameter while holding the others constant) in order to maximize the CSI and determine the optimum threshold values. The following parameter values were determined to be optimal as a result of this exercise:

depth: 1.5 km,
maximum gate-to-gate velocity difference at the 3D detection base: 25 m s^{-1},
maximum gate-to-gate velocity difference anywhere within a 3D detection: 36 m s^{-1}.

Only those 3D detections classified as TVSs were scored.

The scoring results using these optimized parameters applied to the dependent dataset are summarized in Table 3. Overall, the NSSL TDA has a much higher CSI of 29% than either the default or optimized 88D TVS with CSI values of 1% and 11%, respectively. The optimized 88D TVS has a lower POD of 37% compared to the NSSL TDA POD of 40%. The optimized 88D TVS has a much higher FAR of 87% as opposed to a FAR of 47% for the NSSL TDA. Overall, the optimized 88D TVS produced seven times more false alarms than the NSSL TDA. The NSSL TDA also has a relatively higher HSS of 45% than either the optimized or the default 88D TVS with HSS values of 18% and 0%, respectively. The default 88D TVS has a relatively low FAR, but it also has a very low POD since it detects very few vortices. In a case-by-case comparison, the NSSL TDA performed better than the optimized 88D TVS in four (15 April 1994, Houston, Texas; 30 April 1994, Sterling, Virginia; 11 May 1992, Norman, Oklahoma; 2 September 1992, Norman, Oklahoma) out of the six cases. The poorer performance (i.e., relatively higher number of false alarms compared

TABLE 3. Dependent dataset scoring statistics using optimized parameters: numbers of hits (H), misses (M), false alarms (F), and nulls (N); POD, FAR, CSI, and HSS (%); all tornadoes within 150-km range of the radar.

		NSSL TDA				88D TVS (opt.)				88D TVS (def.)			
Date	Radar	H	M	F	N	H	M	F	N	H	M	F	N
15 Apr 1994	Houston, TX	4	2	8	2018	0	6	21	2005	0	6	0	2026
16 Apr 1993	Sterling, VA	4	25	3	2615	19	16	42	2570	1	28	0	2618
30 Apr 1994	Sterling, VA	5	8	11	806	1	13	10	806	0	14	0	816
9 Jun 1994	Memphis, TN	4	21	6	2990	7	16	179	2819	0	23	0	2998
11 May 1992	Norman, OK	39	36	11	913	28	46	34	891	1	68	0	930
2 Sep 1992	Norman, OK	5	1	16	761	4	2	101	676	0	6	1	776
Total		61	93	55	10 103	59	99	387	9767	2	145	1	10 164
		POD	FAR	CSI	HSS	POD	FAR	CSI	HSS	POD	FAR	CSI	HSS
		40	47	29	45	37	87	11	18	1	33	1	0

to number of hits) of the NSSL TDA for the two remaining cases (16 April 1993, Sterling, Virginia; 9 June 1994, Memphis, Tennessee) is attributed in part to range folding that obscured the velocity data at lower elevation angles, especially at the 0.5° elevation angle. Range obscuration may affect the 88D TVS less because detections are not constrained to extend to lower elevation angles, where range folding may be more prevalent. Also, in these two cases, 5 out of the 10 tornadoes had brief lifetimes and occurred along the leading edge of squall lines. Thus, detection of these tornadoes is more difficult.

The scoring results using the optimum parameters from the dependent dataset and applied to the independent dataset are summarized in Table 4. The results are very similar to the scoring results described for the dependent dataset. Overall, the NSSL TDA has POD, FAR, and CSI values of 43%, 48%, and 31%, respectively. In contrast, the optimized 88D TVS has POD, FAR, and CSI values of 37%, 78%, and 16%, respectively. Again, the FAR for the optimized 88D TVS is substantially higher in comparison to the NSSL TDA. It is interesting that the performance results for the NSSL TDA have improved slightly versus the dependent dataset. This may be attributed to less range folding of tornadic vortices as well as the tornado event types contained within the independent dataset. The HSS values are higher for all three algorithms in comparison to the dependent dataset. The NSSL TDA has a much higher HSS value of 46% as compared to 26% and 0% for the optimized and the default 88D TVS, respectively.

It is perhaps deleterious to make general comments regarding algorithm accuracy or skill when a relatively small sample of tornado events is further stratified. However, to offer a more complete picture of algorithm performance, the algorithms have been scored according to region of tornado occurrence and range from the radar.

The scoring results for nonplains versus plains events for the independent dataset are shown in Tables 5 and 6. Very similar results (not shown) also occurred for the dependent dataset. The NSSL TDA has POD, CSI, and HSS values of 68%, 44%, and 59%, respectively, for the plains events. These scores are considerably higher than those for the nonplains events where the POD, CSI, and HSS values are 25%, 20%, and 32%, respectively. Virtually no difference is seen for the default 88D TVS between plains and nonplains events, while the optimized 88D TVS appears to have improved performance for the plains events. Note that once again the optimized 88D TVS is plagued by a significantly higher FAR in comparison to the NSSL TDA, especially for the nonplains events.

The events within each dataset are also stratified by range using two range increments, 0–100 km and 100–150 km. The scores for the dependent dataset are sum-

TABLE 4. Same as Table 3 except independent dataset. The * indicates a nonplains event.

		NSSL TDA				88D TVS (opt.)				88D TVS (def.)			
Date	Radar	H	M	F	N	H	M	F	N	H	M	F	N
15 Apr 1994	St Louis, MO*	2	24	18	1273	8	17	52	1240	0	25	0	1292
5 May 1993	Dodge City, KS	10	12	2	373	5	17	5	370	1	21	0	375
27 Nov 1994	Memphis, TN*	12	26	10	2610	17	22	60	2559	1	35	0	2622
16 Nov 1993	Houston, TX*	15	35	4	2806	9	36	49	2766	2	44	0	2814
9 Apr 1994	Dodge City, KS	35	11	29	1303	21	16	49	1292	1	30	0	1347
28 May 1994	Amarillo, TX	10	3	13	72	5	5	10	78	0	10	0	88
Total		84	111	76	8437	65	113	225	8305	5	165	0	8538
		POD	FAR	CSI	HSS	POD	FAR	CSI	HSS	POD	FAR	CSI	HSS
		43	48	31	46	37	78	16	26	3	0	3	0

TABLE 5. Independent dataset scores for nonplains events: H, M, F, and N represent the numbers of hits, misses, false alarms, and nulls, respectively.

NSSL TDA				88D TVS (opt.)				88D TVS (def.)			
H	M	F	N	H	M	F	N	H	M	F	N
29	85	32	6690	34	71	161	6569	3	104	0	6728
POD	FAR	CSI	HSS	POD	FAR	CSI	HSS	POD	FAR	CSI	HSS
25	52	20	32	32	83	13	21	3	0	3	0

marized in Tables 7 and 8, while scores for the independent dataset are summarized in Tables 9 and 10. Overall, the NSSL TDA performs better than either the default or the optimized 88D TVS. Except for the relatively lower POD (36%) for those tornadoes within 100 km in the dependent dataset, the NSSL TDA has better skill in detecting tornadic vortices compared to both the default and the optimized 88D TVS regardless of range. Note that the optimized 88D TVS has a much larger FAR than the NSSL at both range increments. In the dependent dataset, range folding obscuration is partially responsible for the lower POD of the NSSL TDA for those tornadoes within 100 km of a radar. Note the extremely low scores for the default 88D TVS in both the dependent and independent datasets.

Scoring of the NSSL TDA was also done using range optimized thresholds. The same method that was used to optimize the NSSL TDA for all tornadoes at ranges of 0–150 km was applied to all tornadoes in 50-km range increments from the dependent dataset. Again, the parameter values were chosen based on a maximized CSI. Once the range optimized parameters were obtained, they were applied to the independent dataset. The parameter values and scoring results for both the dependent and independent datasets are depicted in Tables 11 and 12. The NSSL TDA has an overall CSI of 35% and a HSS of 51% for the dependent dataset when the thresholds are varied with range as compared to the CSI and HSS values of 29% and 45%, respectively, when using the optimized parameters for all ranges (Table 3). It is interesting that the parameter value thresholds increase with range. Although it is inconclusive, this may be due to actual radar sampling of strong vortices whose spatial scale is actually larger than the tornado (i.e., mesocyclone). No improvement in POD, FAR, CSI, and HSS is evident in the independent dataset with the range-varied thresholds when compared with using the overall optimized parameters.

5. Evaluation summary

Using a dependent and an independent set of tornadoes, it appears that the NSSL TDA is a significant improvement over the WSR-88D TVS algorithm. The NSSL has a much improved capability of identifying tornadic vortices even though it does produce a number of false alarms. The current 88D TVS using the default adaptable parameters has a very low POD, FAR, CSI, and HSS. However, by significantly lowering the 88D MTA adaptable parameter thresholds improvement in the 88D TVS POD, CSI, and HSS is achieved, but the FAR is also significantly increased.

The NSSL TDA also performs much better on data from plains-type events in comparison to those data from nonplains-type events. However, the data presented here represent only a small sample and more data need to be collected and analyzed to achieve a more reliable evaluation. Even though the NSSL TDA is an overall improvement in comparison to the 88D TVS, there is still room for much improvement.

6. Discussion

The NSSL TDA is designed to detect tornadic vortices regardless of the type of storm (e.g., supercell versus nonsupercell). However, fundamental limitations related to the radar sampling capability may hinder the performance of the NSSL TDA. For example, those detections that are large relative to the size of the radar sample volume, and that occur very near the WSR-88D, may be sampled by more than two adjacent radar beams. This is certainly the case for larger diameter (1–2 km) tornadoes located very close ($<$20 km) to the radar. This is a limiting case for the NSSL TDA since it focuses upon those vortices whose velocity extrema are sampled as gate-to-gate. Also, many tornadoes may form and die within very short periods of time (less than 5 min). Current WSR-88D volume coverage patterns may be

TABLE 6. Same as Table 5 except for plains events.

NSSL TDA				88D TVS (opt.)				88D TVS (def.)			
H	M	F	N	H	M	F	N	H	M	F	N
55	26	44	1747	31	38	65	1739	2	61	0	1810
POD	FAR	CSI	HSS	POD	FAR	CSI	HSS	POD	FAR	CSI	HSS
68	44	44	59	45	68	23	35	3	0	3	0

TABLE 7. Dependent dataset scores for all tornadoes within 0–100 km of a radar: H, M, F, and N represent the numbers of hits, misses, false alarms, and nulls, respectively.

Algorithm	N	H	M	F	POD	FAR	CSI	HSS
NSSL TDA	6103	31	55	26	36	46	28	43
88D TVS (opt.)	5786	46	53	330	46	88	11	17
88D TVS (def.)	6131	1	82	1	1	50	1	0

TABLE 9. Same as Table 7 except independent dataset.

Algorithm	N	H	M	F	POD	FAR	CSI	HSS
NSSL TDA	4866	59	85	54	41	48	30	45
88D TVS (opt.)	4726	56	76	206	42	79	17	26
88D TVS (def.)	4942	4	118	0	3	0	3	0

inadequate to sample a tornadic vortex if tornadogenesis and demise occurs within the time it takes to complete a single volume scan.

Since the NSSL TDA uses a number of thresholds in order to identify tornadic vortices, it is difficult to determine what values to use for a particular event. It is not always clear what type of tornadic event may occur (if at all). For example, setting the depth and strength threshold values too high may result in a low probability of detecting tornadic vortices spawned by minisupercells (Kennedy et al. 1993; Grant and Prentice 1996). On the other hand, isolated supercell outbreaks (those common to the central plains of the United States) may result in an unacceptable number of false alarms if these threshold values are too low. Clearly, proper anticipation of a severe and/or potentially tornadic episode by a forecaster is critical to help determine the optimum threshold values.

It should be recognized that the NSSL TDA does not use certain information that may be useful to determine the tornadic potential of storms. The TDA does not identify reflectivity features such as bounded weak echo regions and/or reflectivity fine lines associated with outflow boundaries, which have been noted as regions where tornadogenesis may occur (Weaver and Nelson 1982; Weaver et al. 1994; Weaver and Purdom 1995). Other important factors that are useful in the tornado warning decision process, but are not considered by the NSSL TDA, include mesoscale model information, satellite data, upper air data (wind and thermodynamic data), surface observations, and spotter reports.

The use of the NSSL TDA output requires more judicious decision making by a forecaster during warning operations because of the significantly greater number of detections in comparison to the 88D TVS. Since the NSSL TDA is not restricted by the performance of any other algorithm, it is capable of identifying tornadic vortices through its own inspection of the velocity data. The NSSL TDA has some added features such as tracking of detections and trending of derived vortex measures that can be invaluable to the decision making process if used properly.

Use of the NSSL TDA as a self-sufficient means upon which to solely base a tornado warning would be a misuse of its merits. Instead, the NSSL TDA should be regarded as an added and complementary guidance tool in the tornado warning decision process. The WSR-88D and its attendant algorithms should be used in conjuction with a forecaster's knowledge of the current and forecast conditions of the atmosphere (Brooks et al. 1994; Doswell et al. 1993; Moller et al. 1994). Proper anticipation of a tornadic event by the forecaster is imperative in the tornado warning decision process. Thus, intimate knowledge of the current and evolving conditions of the atmosphere, understanding of conceptual models related to tornadic storms, and the environments within which they form is paramount to timely and accurate tornado warnings.

Current plans for continued development of the NSSL TDA include the addition of a neural network that will be trained using the various output information from the NSSL TDA. Some promising work in the use of neural networks associated with the NSSL Mesocyclone Detection Algorithm (NSSL MDA) (Stumpf et al. 1998) has been completed. It has been shown that a neural network can enhance the capability of diagnosing vortices identified by the NSSL MDA as either tornadic, severe, nontornadic, or nonsevere (Marzban and Stumpf 1996). A database consisting of output from the NSSL TDA and MDA that will be used to train three neural networks: NSSL MDA input only, NSSL TDA input only, and combined NSSL MDA/TDA input. Furthermore, the NSSL TDA has been accepted by the WSR-88D OSF to be implemented into build 10 of the WSR-88D Radar Products Generator (RPG). However, the build 10 TDA will not include tracking of detections and trending of their attributes. The implementation work will continue into the summer of 1998 when build 10 is scheduled to be installed into the WSR-88D RPG.

Perhaps more importantly, we plan to begin work on incorporating the various techniques from the NSSL MDA and TDA and other sources into a new algorithm

TABLE 8. Same as Table 7 except for all tornadoes within 100–150 km of a radar.

Algorithm	N	H	M	F	POD	FAR	CSI	HSS
NSSL TDA	4000	30	38	29	44	49	31	46
88D TVS (opt.)	3981	13	46	57	22	81	11	19
88D TVS (def.)	4033	1	63	0	2	0	2	0

TABLE 10. Same as Table 8 except for independent dataset.

Algorithm	N	H	M	F	POD	FAR	CSI	HSS
NSSL TDA	3571	25	26	22	49	47	34	50
88D TVS (opt.)	3579	9	37	19	20	68	14	24
88D TVS (def.)	3596	1	47	0	2	0	2	0

TABLE 11. Dependent dataset scores for the NSSL TDA using range optimized parameters: depth, velocity difference at the 0.5° elevation angle ($DV_{0.5°}$), and maximum velocity difference withi a 3D detection (DV_{max3D}). Here H, M, F, and N represent the numbers of hits, misses, false alarms, and nulls, respectively.

Range (km)	Depth (km)	$DV_{0.5°}$ (m s^{-1})	DV_{max3d} (m s^{-1})	N	H	M	F	POD	FAR	CSI	HSS
0–50	1.5	16	26	2351	20	21	10	49	33	39	56
50–100	3.0	25	36	3754	19	26	14	42	42	32	48
100–150	3.9	26	44	4012	29	39	17	43	37	34	50
Total				10 117	68	86	41	44	38	35	51

to be called the Vortex Detection and Diagnosis Algorithm (VDDA). This algorithm is based upon the paradigm that the various detection and diagnosis techniques be interdependent as opposed to the current dependence of 88D TVS on the WSR-88D Mesocyclone Detection Algorithm (NEXRAD 1985), and the case for build 10 where the NSSL TDA will operate independently of any other algorithms. It is anticipated that the VDDA will provide more accurate and useful information to the field forecaster in warning operations by utilizing various vortex detection and diagnosis techniques (e.g., neural networks) cohesively to provide the most useful guidance information, that is, derived measures and probabilistic information, to the forecaster. Finally, ongoing analysis of the data collected during the field phase of the Verification of the Origins of Rotation in Tornadoes Experiment (Rasmussen et al. 1994) and other investigations related to tornadic vortices (Trapp and Mitchell 1995) will, hopefully, add to our understanding of severe storms and tornadoes and, as a result, enhance the development of future severe storm and tornado detection, diagnostic and prognostic algorithms.

Acknowledgments. Thanks are extended to Dr. R. Jeffrey Trapp and Mr. Bill Conway for graciously reviewing an early version of this manuscript. We gratefully acknowledge the gracious support provided by the WSR-88D Operational Support Facility and the Federal Aviation Administration in the development of the NSSL TDA. Other contributors toward the development of the NSSL TDA include Bim Wood (NSSL) and Rodger Brown (NSSL). Robert R. Lee, W. David Zittel, Mark Fresch, and Tim O'Bannon also contributed to the development of the NSSL TDA. Administrative support was provided by Kelly Lynn (NSSL). Others who helped with gathering the radar and ground truth information include Karen Cooper and Chris Robbins. Kurt Hondl (NSSL) developed a display system that allowed for the analysis of much of the WSR-88D base velocity data. Thanks are extended to all of the individuals not specifically mentioned in this manuscript for their ideas and comments, and the anonymous reviewers for their enlightening comments that further honed the quality of this manuscript.

APPENDIX

Important NSSL TDA Parameters

Minimum required shear segment velocity difference: 11 m s^{-1}
Minimum number of shear segments for a 2D detection: three
Maximum aspect ratio (radial diameter/azimuthal diameter): 4
Minimum required number of 2D detections to declare a 3D detection: three
Minimum required depth for a 3D detection to declare a TVS or ETVS: 1.5 km
Minimum base height for TVS detection: 0.5° or below 600 m ARL
Minimum velocity difference required at the base *or* at any level within a 3D detection to declare a TVS or ETVS: 25 m s^{-1} and 36 m s^{-1}, respectively.

Select WSR-88D MTA adaptable parameters (relaxed)

High momentum = 180 km^2 h^{-1}
High shear = 7.2 h^{-1}
Low momentum = 90 km^2 h^{-1}
Low shear = 3.6 h^{-1}
Pattern vector = 6
TVS shear = 18 h^{-1}.

TABLE 12. Same as Table 11 except independent dataset.

Range (km)	Depth (km)	$DV_{0.5°}$ (m s^{-1})	Dv_{max3d} (m s^{-1})	N	H	M	F	POD	FAR	CSI	HSS
0–50	1.5	16	26	1496	30	30	27	50	47	35	49
50–100	3.0	25	36	3369	32	52	28	38	47	29	43
100–150	3.9	26	44	3576	17	34	17	33	50	25	39
Total				8441	79	116	72	41	48	30	45

REFERENCES

Austin, G., 1945: Radar storm detection. *Weather Service Bulletin*, Vol. 3, No. 7, Army Air Force, 12–19.

Bieringer, P., and P. S. Ray, 1996: A comparison of tornado warning lead times with and without NEXRAD Doppler radar. *Wea. Forecasting*, **11,** 47–52.

Bigler, S. G., 1955: An analysis of tornado and severe weather echoes. Preprints, *Fifth Conf. on Radar Meteorology*, Asbury Park, NJ, Amer. Meteor. Soc., 167–175.

——, 1956: A note on the successful identification and tracking of a tornado by radar. *Weatherwise*, **9,** 198–201.

Brady, R. H., and E. J. Szoke, 1989: A case study of nonmesocyclone tornado development in northeast Colorado: Similarities to waterspout formation. *Mon. Wea. Rev.*, **117,** 843–856.

Brooks, H. E., C. A. Doswell III, and J. Cooper, 1994: On the environments of tornadic and nontornadic mesocyclones. *Wea. Forecasting*, **9,** 606–618.

Brown, R. A., W. C. Bumgarner, K. C. Crawford, and D. Sirmans, 1971: Preliminary Doppler velocity measurements in a developing radar hook echo. *Bull. Amer. Meteor. Soc.*, **52,** 1186–1188.

——, L. R. Lemon, and D. W. Burgess, 1978: Tornado detection by pulsed Doppler radar. *Mon. Wea. Rev.*, **106,** 29–38.

Browning, K. A., 1965: The evolution of tornadic storms. *J. Atmos. Sci.*, **22,** 664–668.

Burgess, D. W., L. R. Lemon, and R. A. Brown, 1975: Tornado characteristics revealed by Doppler radar. *Geophys. Res. Lett.*, **2,** 183–184.

——, R. J. Donaldson Jr., and P. R. Desrochers, 1993: Tornado detection and warning by radar. *The Tornado: Its Structure, Dynamics, Prediction, and Hazards*, *Geophys. Monogr.*, No. 79, Amer. Geophys. Union, 203–221.

Conway, J. W., K. D. Hondl, M. J. Moreland, J. M. Cordell, and R. J. Harron, 1995: Improvements in the WSR-88D dealiasing algorithm: The pursuit of the final, most important gate. Preprints, *27th Conf. on Radar Meteorology*, Vail, CO, Amer. Meteor. Soc., 145–147.

Crum, T. D., and R. L. Alberty, 1993: The WSR-88D and the WSR-88D Operational Support Facility. *Bull. Amer. Meteor. Soc.*, **74,** 1669–1687.

Donaldson, R. J., Jr., 1970: Vortex signature recognition by a Doppler radar. *J. Appl. Meteor.*, **9,** 661–670.

Doswell, C. A., III, S. J. Weiss, and R. H. Johns, 1993: Tornado forecasting: A review. *The Tornado: Its Structure, Dynamics, Prediction, and Hazards*, *Geophys. Monogr.*, No. 79, Amer. Geophys. Union., 557–571.

Easterbrook, C. C., 1967: Some Doppler radar measurements of circulation patterns in convective storms. *J. Appl. Meteor.*, **6,** 882–888.

Forbes, G. S., 1981: On the reliability of hook echoes as tornado indicators. *Mon. Wea. Rev.*, **109,** 1457–1466.

Freund, R. F., 1966: Radar echo signature of tornadoes. Preprints, *12th Conf. on Radar Meteorology*, Norman, OK, Amer. Meteor. Soc., 362–365.

Fujita, T., 1958: Mesoanalysis of the Illinois tornadoes of 9 April 1953. *J. Meteor.*, **15,** 288–296.

Grant, B., and R. Prentice, 1996: Mesocyclone characteristics of minisupercell thunderstorms. Preprints, *15th Conf. on Weather Analysis and Forecasting*, Norfolk, VA, Amer. Meteor. Soc., 362–365.

Howard, K., J. J. Gourley, and R. A. Maddox, 1997: Uncertainties in WSR-88D measurements and their impacts on monitoring thunderstorm life cycles. *Wea. Forecasting*, **12,** 166–174.

Johnson, J. T., and Coauthors, 1995: Operations testing of enhanced WSR-88D algorithms and display concepts in National Weather Service Offices. Preprints, *27th Conf. on Radar Meteorology*, Vail, CO, Amer. Meteor. Soc., 170–172.

——, P. L. MacKeen, A. Witt, E. D. Mitchell, G. J. Stumpf, M. D. Eilts, and K. W. Thomas, 1998: The Storm Cell Identification and Tracking (SCIT) algorithm: An enhanced WSR-88D algorithm. *Wea. Forecasting*, **13,** 263–276.

Kennedy, P. C., N. E. Westcott, and R. W. Scott, 1993: Single Doppler radar observations of a minisupercell tornadic thunderstorm. *Mon. Wea. Rev.*, **121,** 1860–1870.

Klazura, G. E., and D. A. Imy, 1993: A description of the initial set of analysis products available from the NEXRAD WSR-88D system. *Bull. Amer. Meteor. Soc.*, **74,** 1293–1311.

Kraus, M. J., 1973: Doppler radar observations of the Brookline, Massachusetts tornado of 9 August 1972. *Bull. Amer. Meteor. Soc.*, **54,** 519–524.

Lhermitte, R. M., 1969: Doppler radar observation of a convective storm. Preprints, *Sixth Conf. on Severe Local Storms*, Chicago, IL, Amer. Meteor. Soc., 139–145.

Marzban, C., 1998: Scalar measures of performance in rare-event situations. *Wea. Forecasting*, in press.

——, and G. J. Stumpf, 1996: A neural network for tornado prediction based on Doppler radar-derived attributes. *J. Appl. Meteor.*, **35,** 617–626.

Mitchell, E. D., 1995: An enhanced NSSL tornado detection algorithm. Preprints, *27th Conf. on Radar Meteorology*, Vail, CO, Amer. Meteor. Soc., 406–408.

——, and G. J. Stumpf, 1996: The 19 April 1995 Fort Worth/Dallas tornado event: Implications for automated vortex recognition. Preprints, *18th Conf. on Severe Local Storms*, San Francisco, CA, Amer. Meteor. Soc., 574–576.

Moller, A. R., C. A. Doswell III, M. P. Foster, and G. R. Woodall, 1994: The operational recognition of supercell thunderstorm environments and storm structures. *Wea. Forecasting*, **9,** 327–347.

NCDC, 1992–94: *Storm Data.* Vols. 34–36. [Available from the National Climatic Data Center, Federal Building, Asheville, NC, 28801-2696.]

Polger, P. D., B. S. Goldsmith, R. C. Przywarty, and J. R. Bocchieri, 1994: National Weather Service warning performance based on the WSR-88D. *Bull. Amer. Meteor. Soc.*, **75,** 203–214.

Rasmussen, E. N., J. M. Straka, R. Davies-Jones, C. A. Doswell III, F. H. Carr, M. D. Eilts, and D. R. MacGorman, 1994: Verification of the Origins of Rotation in Tornadoes Experiment: VORTEX. *Bull. Amer. Meteor. Soc.*, **75,** 995–1006.

Sadowski, A., 1969: Size of tornado warning area when issued on basis of radar hook echo. ESSA Tech. Memo. WBTM Fcst 10, 26 pp. [NTIS PB 184613.]

Smith, R. L., and D. W. Holmes, 1961: Use of Doppler radar in meteorological observations. *Mon. Wea. Rev.*, **89,** 1–7.

Stout, G. E., and F. A. Huff, 1953: Radar records Illinois tornadogenesis. *Bull. Amer. Meteor. Soc.*, **34,** 281–284.

Stumpf, G. J., and D. W. Burgess, 1993: Observations of lower-tropospheric misocyclones along the leading edge of a bow echo thunderstorm. Preprints, *26th Int. Conf. on Radar Meteorology*, Norman, OK, Amer. Meteor. Soc., 215–217.

——, and M. P. Foster, 1996: The 1995 NSSL warning decision support system test at the Fort Worth National Weather Service Forecast Office. Preprints, *18th Conf. on Severe Local Storms*, San Francisco, CA, Amer. Meteor. Soc., 570–573.

——, A. Witt, E. D. Mitchell, P. L. Spencer, J. T. Johnson, M. D. Eilts, K. W. Thomas, and D. W. Burgess, 1998: The National Severe Storms Laboratory Mesocyclone Detection Algorithm for the WSR-88D. *Wea. Forecasting*, **13,** 304–326.

Trapp, R. J., and E. D. Mitchell, 1995: Characteristics of tornadic vortex signatures detected by WSR-88D radar. Preprints, *27th Conf. on Radar Meteorology*, Vail, CO, Amer. Meteor. Soc., 211–212.

Vasiloff, S. V., 1992: Comparison of several mesocyclone and tornado detection algorithms. OSF Rep., 50 pp. [Available from National Weather Service Operational Support Facility, 1200 Westheimer Dr., Norman, OK 73069.]

——, 1993: Single-Doppler radar study of a variety of tornado types. *The Tornado: Its Structure, Dynamics, Prediction, and Hazards*, *Geophys. Monogr.*, No. 79, Amer. Geophys. Union, 223–231.

Wakimoto, R. M., and J. W. Wilson, 1989: Nonsupercell tornadoes. *Mon. Wea. Rev.*, **117,** 1113–1140.

——, and J. K. Lew, 1993: Observations of a Florida waterspout during CaPE. *Wea. Forecasting,* **8,** 412–423.

Weaver, J. F., and S. P. Nelson, 1982: Multiscale aspects of thunderstorm gust fronts and their effects on subsequent storm development. *Mon. Wea. Rev.*, **110,** 707–718.

——, and J. F. W. Purdom, 1995: An interesting mesoscale storm–environment interaction observed just prior to changes in severe storm behavior. *Wea. Forecasting,* **10,** 449–453.

——, ——, and E. J. Szoke, 1994: Some mesoscale aspects of the 6 June 1990 Limon, Colorado, tornado case. *Wea. Forecasting,* **9,** 45–61.

Wells, F. E., 1963: An observation of an anticyclonic hook-shaped echo in an area of known tornadic activity. *Proc. 10th Weather Radar Conf.*, Washington, DC, Amer. Meteor. Soc., 62–67.

Wilks, D. S., 1995: *Statistical Methods in the Atmospheric Sciences.* Academic Press, 467 pp.

Witt, A., M. D. Eilts, G. J. Stumpf, E. D. Mitchell, J. T. Johnson, and K. W. Thomas, 1998: Evaluating the performance of WSR-88D severe storm detection algorithms. *Wea. Forecasting,* **13,** 513–518.

Wood, V. T., and R. A. Brown, 1997: Effects of radar sampling on single-Doppler velocity signatures of mesocyclones and tornadoes. *Wea. Forecasting,* **12,** 928–938.

Zrnic, D. S., and R. J. Doviak, 1975: Velocity spectra with a pulse-Doppler radar. *J. Appl. Meteor.*, **14,** 1531–1539.